Origin of compaction bands: Theory and numerical models

Alexandre I. Chemenda

Géosciences Azur, Université de Nice-Sophia Antipolis, CNRS, 250 Rue Albert Einstein, 06560 Valbonne, France.

Summary

Based on the theoretical analysis and finite-difference simulations we show that tabular compaction bands can be initiated as constitutive instabilities resulting from the deformation bifurcation. After initiation, some bands are rapidly dying, while others continue to evolve accumulating the inelastic deformation/damage and resulting in the band propagation and thickening. This process occurs in three stages and is more complicated than what follows from the LEFM anti-crack model. The band propagation distance is proportional to the initial (resulted from the bifurcation) band length that in turn is proportional to the hardening modulus h and theoretically can reach infinity when h reaches certain critical value.

1. Introduction

After the discovery of compaction bands in the field (Mollema and Antonellini, 1996), there has been a growing amount of studies of these features based on the theoretical analysis (e.g., Issen and Rudnicki, 2000; Sternlof et al., 2005; Chemenda, 2009), numerical modeling (Katsman et al., 2005; Wang et al., 2008; Chemenda, 2009), and the rock testing (e.g., Wong et al., 1997; Olsson and Holcomb, 2000; Baud et al., 2004). The possibility of formation of this type of localization bands has been predicted in the frame of the continuous bifurcation analysis (Ottosen and Runesson, 1991; Perrin and Leblond, 1993; Issen and Rudnicki, 2000), which then has been extended to the next, discontinuous bifurcation step when the elastic-plastic loading continues only within the tabular band set, while outside the bands the material undergoes elastic unloading (Chemenda, 2009). The finite-difference numerical simulations confirmed this result and reproduced both zigzag shape of the bands generated in the laboratory tests (Fig. 1a) and their progressive appearance from the sample (numerical model) ends (where the compressive load is applied) toward the middle (Fig. 1b).

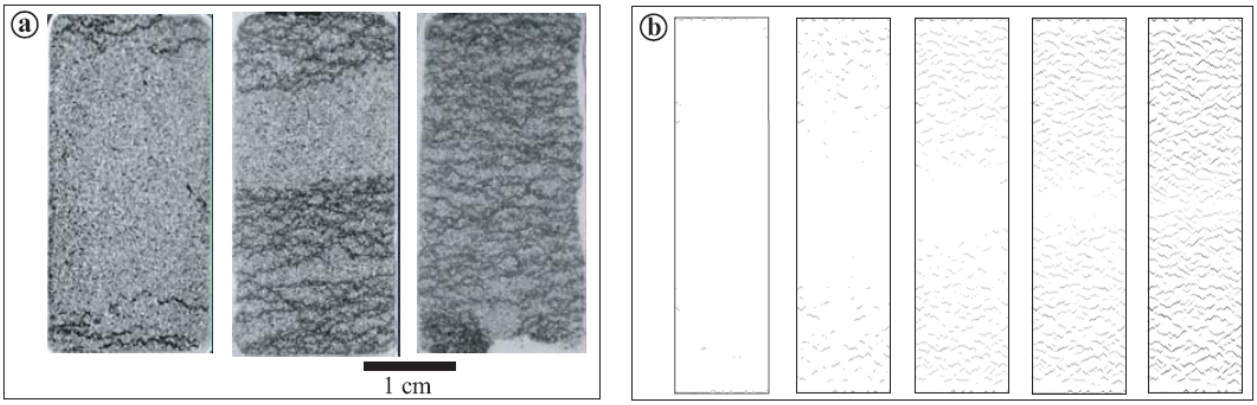

Fig. 1. (a) Discrete compaction banding in Bentheim sandstone sample under vertical axisymmetric compression at different axial strains (from Baud at al. (2004)); (b) Patterns of accumulated inelastic equivalent shear deformation $\overline{\gamma}^{p}$ for successive stages of the evolution of numerical model under axisymmetric compression stress (from (Chemenda, 2009)).

Such a propagation of the deformation (of its appearance) in the direction perpendicular to the bands is caused by the boundary effect and is related to the evolution of the material constitute properties with deformation (Chemenda, 2009). Thus a constitutive instability seems to be rather a plausible mechanism of compaction banding generated in the laboratory experiments. The problem is that the natural (geological) compaction bands have a different aspect. In most cases they are rather linear (planar) and are organized in regular tabular sets. The size of the bands (their thickness d and length L) can vary in large limits (e.g., Sternlof et al., 2005) and is much larger than that of the "experimental" bands, which might suggest different formation mechanisms. In this work we show that the difference between experimental and natural bands can be explained by the difference in the constitutive response, which depends not only on the material properties, but also on the size of the structure (laboratory sample *vs* geological object).

2. Summary of the results of multi-band discontinuous bifurcation analysis

The average spacing λ_0 between compaction bands resulted from the discontinuous bifurcation is (Chemenda, 2009)

$$\lambda_0 = \frac{d_0\left[18(h-h_{cr}^c)(2\nu-1)(\nu-1)+C_{\alpha\beta}\right]}{18(h-h_{cr}^c)(2\nu-1)(1-\nu)},\quad h_{cr}^c = \frac{(1+\nu)(\beta-\alpha)^2}{9(1-\nu)} - \frac{1+\nu}{1-\nu}\left(\frac{1}{2}N_3 - \frac{\alpha+\beta}{3}\right)^2 - (1-\frac{3}{4}N_3^2) \quad (1)$$

where $C_{\alpha\beta} = \left[2\beta(1+\nu)-3N_3(2\nu-1)\right]\left[2\alpha(1+\nu)-3N_3(2\nu-1)\right]$, α is the internal friction coefficient, β is the dilatancy factor, ν is the Poisson's ratio, h is the normalized hardening modulus, h_{cr}^c is the normalized critical hardening modulus at which $\lambda_0 = \infty$ or the spacing parameter $\chi = d_0/\lambda_0$ is zero, d_0 is the band thickness at bifurcation, $N_3 = \frac{s_3}{\bar{\tau}} = -\frac{1}{2}(N + \frac{1}{2}\sqrt{4-3N^2})$, $N = -s_2/\bar{\tau}$ is the stress-state parameter, s_2 is the intermediate principal deviatoric stress, $\bar{\tau}$ is the Mises equivalent shear stress, "*c*" stands for compaction.

Condition (1) applies when $h^c(\chi) \geq h^{sh}(\chi)$, i.e., when the constitutive instability occurs in the form of compaction banding (otherwise it will occur via shear banding). $h^c(\chi)$ follows from (1) ($h^c(\chi) = h(\chi)$), $h^{sh}(\chi)$ corresponds to shear localization banding and represents very cumbersome expression from (Chemenda, 2007).

Fig. 2 shows examples of $h^c(\chi)$ and $h^{sh}(\chi)$ curves. The coordinates of their intersection point (IP) are defined by the constitutive and stress-state parameter values. The IP itself defines the domains with different regimes of deformation localization. Compaction banding occurs when the stress-state point (SP) is located to the right of the IP (i.e., when $h^c(\chi) > h^{sh}(\chi)$, Fig. 2). If the SP is to the left of the IP (i.e., $h^c(\chi) < h^{sh}(\chi)$), shear banding occurs.

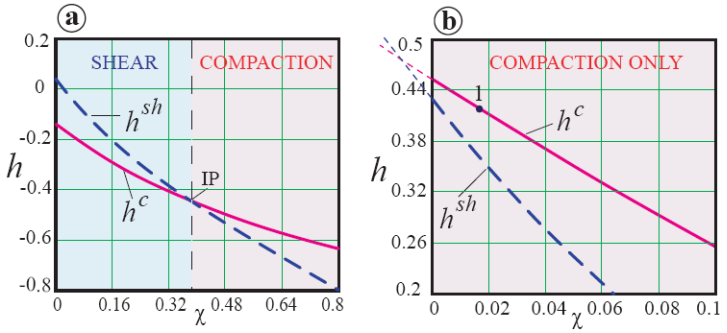

Fig. 2. Hardening moduli for compaction (h^c) and shear (h^{sh}) banding versus spacing parameter χ for $\alpha = -0.22$, $\nu = 0.25$, $N = 0.277$ and different β values: (a) β = -0.7, (b) β = -2. Point 1 corresponds to the numerical model in Fig. 4.

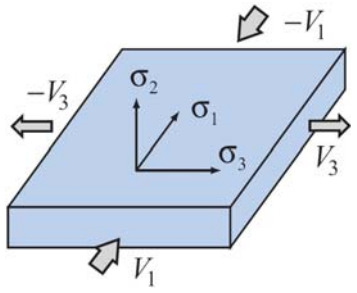

Fig. 3. Setup of numerical models. Model parameters correspond to p. 1 in Fig. 2b. The horizontal boundaries are fixed in the vertical direction. All boundaries are free in the direction parallel to the boundaries.

The numerical analysis of bifurcation shows (Chemenda, 2009) that the transition between two banding modes is gradual and corresponds to the formation of zigzag bands (Fig. 1b) like in the rock tests, Fig. 1a (the bands are zigzag, but their general/average trend is orthogonal to σ_1, $\sigma_1 > \sigma_2 > \sigma_3$, the compressive stress is positive). The further the SP is located to the right in Fig. 2 (e.g., the higher is the β value), the denser will be the compaction band set and the shorter will be the linear segments composing the bands. On the other hand, the closer the IP abscissa (χ) is to zero (or the closer the ordinate of IP is to h_{cr}^c), the larger are both the compaction band spacing λ_0 and the length L_0 when the SP is located not far to the right of the IP (at $h = h_{cr}^c$ $\lambda_0 = \infty$, eq. (1)). A shift of the IP to the left occurs for example when β decreases (at other parameter values fixed), Fig. 2. These conditions (when h approaches h_{cr}^c and the SP is not far to right of the IP) correspond to the formation of a tabular set of long parallel bands like those observed in geological outcrops.

The bifurcation analysis predicted this result deals only with the onset of localization deformation when inelastic deformation/damage within the bands is infinitesimal. The bands observed in the outcrops result from the post-bifurcation band evolution when inelastic deformation is finite. This process can be investigated only experimentally (on the properly scaled physical models) or on the dynamic numerical models like those presented below.

3. Numerical modeling

2-D numerical simulations were performed using dynamic, finite-difference, time-matching explicit code Flac3D. The Drucker-Prager model (the same as in the above theory) with strain softening and β variation with $\bar{\gamma}^p$ was implemented in this code. The boundary conditions are shown in Fig. 3 and the result of one of the typical simulations in Fig. 4. In this model *h* is set to 0.41 close to h_{cr}^c (point 1 in Fig 2b), which for the chosen other parameter values is 0.454 (as follows from (1)).

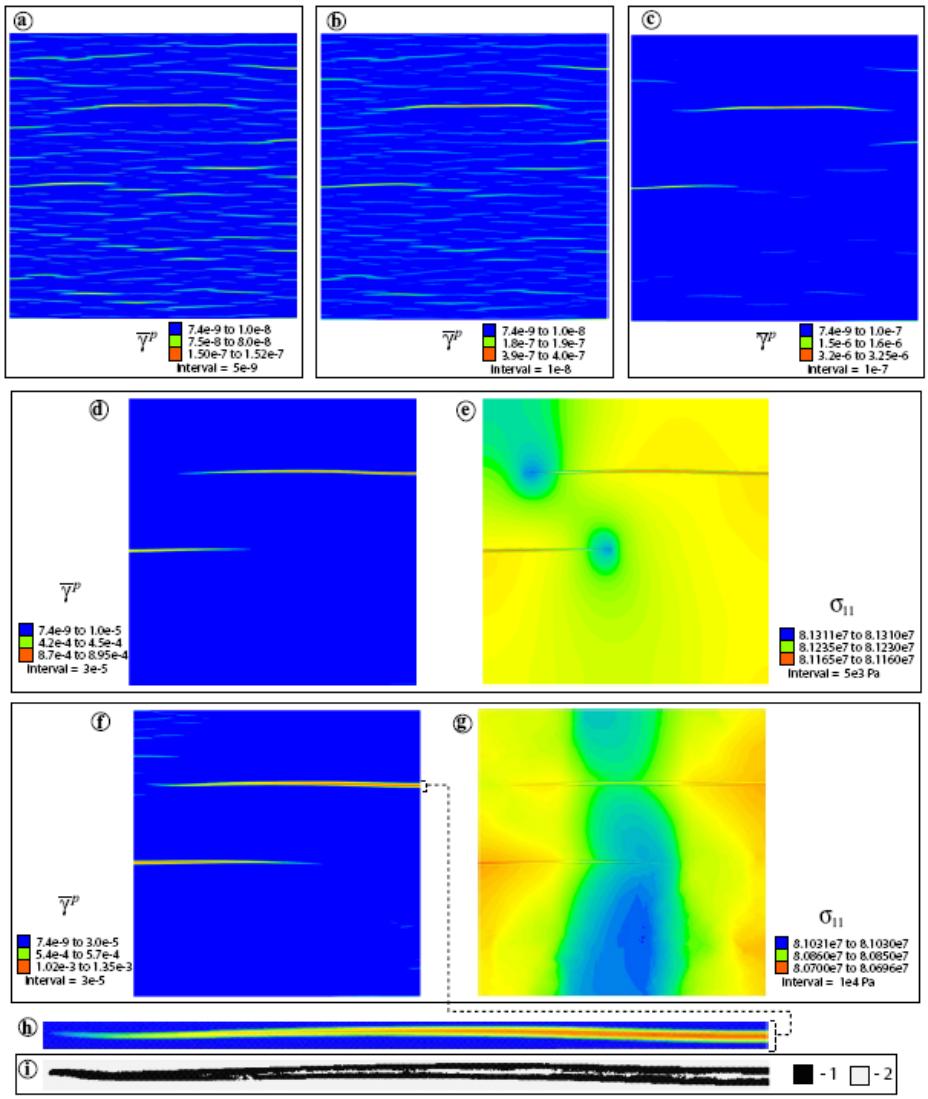

Fig. 4

Evolution of $\bar{\gamma}^p$ and σ_{11} in the model with parameters corresponding to point 1 in Fig. 2b. σ_{11} is the normal stress in x_1 direction. (d) – (e), (f) – (g) correspond, respectively, to the same deformation stages. (h) Zoom of the upper band in (f); (i) The same band shown in terms of the mechanical response of the material: 1, Elastic-plastic response; 2, Elastic response. The inelastic deformation is concentrated along the band perimeter (Fig. 4i), while the response of the already compacted "core" part of the band is mostly elastic. The maximal band thickness *d* is equal to 12 numerical zone sizes and continue growing with further model cycling. Considering that the model is free to move parallel to the boundaries, they are axes of symmetry. Therefore the bands "cut" by the boundaries represent the halves of the entire bands. The model size is 1×1 m^2 (500×500 numerical zones).

The bifurcation occurs at a very small $\bar{\gamma}^p$ and results in the formation of a sub-parallel set of compaction bands orthogonal to σ_1 (Fig. 4a) as is assumed in the above theory. Then in some bands $\bar{\gamma}^p$ increases, while in others (the dying ones) the inelastic deformation ceases, Fig. 4b. The distribution of the stresses at this stage is practically uniform. The evolution of the band pattern reaches an intermediate stationary stage (corresponding to Figs. 4b, c), during which $\bar{\gamma}^p$ increases in the bands remaining active, while L_0 and d_0 remain constant (d_0 is equal to 4–5 numerical zone sizes). Then some bands start propagating rapidly (the band length increases

from initial value L_0 to L), while in others the inelastic deformation ceases (Fig. 4d). At this stage a small (less than 0.1% of the average/background stress value) concentration of σ_{11} is observed at the bands tips (Fig. 4e). Then the band propagation slows down simultaneously with the acceleration of the band thickening, which occurs by incorporating the "intact" (not compacted yet) material at the bands margins. In Figs. 4f, h the propagation is already practically stopped and only band thickening continuous. The inelastic deformation is concentrated along the band perimeter, while the response of the already compacted "core" part of the band is mostly elastic (Fig. 4i). At this stage no stress concentration exists at all (Fig. 4g).

Reduction of h (compared to the value in the presented model) results in the reduction of final band spacing λ, while h increase causes λ to grow in accordance with the theoretical prediction. The average band length L increases, while the aspect ratio d/L reduces and theoretically reaches zero at $h = h_{cr}^c$. At $h > h_{cr}^c$ the deformation localization does not occur, as is predicted by theory and confirmed by the numerical modeling.

Increase in β results in both the curvature of the compaction bands and reduction of the band spacing (as in Fig. 1b)

5. Concluding discussion

Very small (close to zero) aspect ratio of natural bands in the Aztec sandstone (Sternlof et al., 2005) implies that the bifurcation in this region occurred at h close to h_{cr}^c, i.e., to the maximal value at which the bifurcation is possible. This suggests also that the evolution (reduction) of h with deformation was rather smooth (h close to h_{cr}^c was reached smoothly). In other words, the grain compaction occurred "quietly" without abrupt accelerations that could be caused by intense grain crushing typical of compaction bands generated in the laboratory tests (e.g., Wong et al., 1997). Such a crushing and associated pore collapse may result in a discontinuous evolution of h, its drop before reaching h_{cr}^c, and formation of dense bands as is followed from eq. (1) and observed both in the rock mechanics tests and numerical models (Fig. 1). The above difference in "geological" and "experimental" compaction banding can be explained by the fact that the tested rocks are typically moderately- to strongly-cemented, while cementation of the Aztec sandstone is either very weak or inexistent (Sternlof et al., 2005).

The small size of the rock samples certainly also plays a role. The height of the samples is several centimeters, which is much less than the spacing of the bands in the field (tens of centimeters). The long and straight bands that necessarily should have large spacing (χ close to zero), simply cannot be formed in the small samples where the localization can occur only at $h < h_{cr}^c$. If h reduces smoothly (after reaching its peak value) during loading, only one (or two symmetric) band (bands) can be initiated at the sample end (ends). These bands will then thicken to progressively fill the entire sample. Such a process was obtained both in the rock tests (e.g., Olsson and Holcomb, 2000; Baud et al., 2000) and numerical models (Chemenda, 2009). If h evolves discontinuously and reduces abruptly well before reaching h_{cr}^c, a dense set of bands will be formed as discussed above.

The band propagation distance in the model increases with L_0 (which in turn is the larger, the closer is h to h_{cr}^c), i.e., the longer band propagates easier. This is where the behavior of the compaction bands is similar to the crack (in this case "anticrack") propagation, which occurs due to the stress concentration at the crack tips. The similarity however does not go beyond this, as stress concentration in Fig. 4e is very small (negligible), the band growth occurs in three distinctive stages and involves the inelastic deformation not only at the band tips, but within the whole band.

References

Baud, P., Klein, E., Wong, T.-f., 2004. J. Struct. Geol. 26, 603–624.
Chemenda, A. I., 2007. J Geophys. Res. 112, B11404, doi:10.1029/2007JB005026.
Chemenda, A. I., 2009. J. Mech. Phys. Solids 57, 851-868.
Issen, K.A., Rudnicki, J.W., 2000. J. Geophys. Res. 105, 21,529-21,536.
Mollema, P.N., Antonellini, M.A., 1996. Tectonophysics 267, 209–228.
Olsson, W. A., Holcomb, D. J., 2000. Lett. 27, 3537– 3540.
Ottosen, N.S., Runesson, K., 1991. Int. J. Solids Struct. 27, 401-421.
Perrin, G., Leblond, J.B., 1993, J. Appl. Mech. 60, 842-846.
Sternlof, K., Rudnicki, J. W., Pollard, D. D., 2005. J. Geophys. Res. 110, B11403, doi:10.1029/2005JB003764.
Wong, T.-f., David, C., Zhu, W., 1997. J. Geophys. Res. 102, 3009-3025.